nanomaterials

MDPI

Article

Constructing Co_3O_4/g-C_3N_4 Ultra-Thin Nanosheets with Z-Scheme Charge Transfer Pathway for Efficient Photocatalytic Water Splitting

Yuan Guo, Wanqing Liu, Wei Duan, Siyu Wang, Liqun Jia, Guoqing Zhang, Baolin Zhu, Weiping Huang and Shoumin Zhang *

Department of Chemistry, Key Laboratory of Advanced Energy Material Chemistry (MOE), TKL of Metal and Molecule Based Material Chemistry, Nankai University, Tianjin 300071, China; 2120190685@mail.nankai.edu.cn (Y.G.); 2120200715@mail.nankai.edu.cn (W.L.); dduan0417@163.com (W.D.); siyu2142021@163.com (S.W.); jlq15064153315@163.com (L.J.); zhangguoqing9401@163.com (G.Z.); zhubaolin@nankai.edu.cn (B.Z.); hwp914@nankai.edu.cn (W.H.)

* Correspondence: zhangsm@nankai.edu.cn

Abstract: Photocatalytic water splitting for hydrogen generation is a significant pathway for sustainable energy conversion and production. The photocatalysts with a Z-scheme water splitting charge transfer pathway is superior due to the good separation and migration ability of photoexcited charge carriers. Herein, Co_3O_4/g-C_3N_4 photocatalysts with Z-scheme charge transfer pathway were successfully constructed by an electrostatic interaction-annealing method. The as-prepared Co_3O_4/g-C_3N_4 ultra-thin nanosheets were tested and analyzed by XRD, EA, ICP, SEM, TEM, AFM, XPS, UV-Vis DRS, PL and photoelectrochemical measurements. Moreover, the influences of fabrication parameters on performance of Co_3O_4/g-C_3N_4 catalysts were investigated, and 0.5% Co_3O_4/g-C_3N_4 exhibited the optimal activity. Based on the characterization and catalytic performance, the Z-scheme charge transfer pathway of Co_3O_4/g-C_3N_4 was established and put forward. To further improve the catalytic performance of Co_3O_4/g-C_3N_4, 0.5% Pt was added as a co-catalyst. The obtained Pt/0.5% Co_3O_4/g-C_3N_4 was recyclable and remained the original catalytic water splitting performance within 20 h. The modification of Co_3O_4 and Pt improved the separation and migration of e^- and h^+, and induced the increased hydrogen evolution rate of g-C_3N_4.

Keywords: Co_3O_4/g-C_3N_4 ultra-thin nanosheets; Z-scheme charge transfer pathway; photocatalytic; water splitting; H_2 evolution

Citation: Guo, Y.; Liu, W.; Duan, W.; Wang, S.; Jia, L.; Zhang, G.; Zhu, B.; Huang, W.; Zhang, S. Constructing Co_3O_4/g-C_3N_4 Ultra-Thin Nanosheets with Z-Scheme Charge Transfer Pathway for Efficient Photocatalytic Water Splitting. *Nanomaterials* **2021**, *11*, 3341. https://doi.org/10.3390/nano11123341

Academic Editor: Yuichi Negishi

Received: 12 November 2021
Accepted: 7 December 2021
Published: 9 December 2021

1. Introduction

Photocatalytic hydrogen generation is a high efficiency, environmentally friendly and economically practical technology for utilizing solar energy [1–3]. It promises a sustainable alternative via semiconductors to address environmental issues and energy shortages all around the world [4–6]. The strong optical absorption ability, high separation and migration efficiency and stability are major factors for the photocatalysts' activity for hydrogen evolution [7,8]. Now efforts have been devoted to fabricating more and more effective semiconductors for solar-energy utilization and conversion, majorly categorized as metal oxides, amorphous (oxy)-hydroxides, (oxy)nitrides, (oxy)sulphides and polymeric catalysts [9,10].

Graphitic carbon nitride (g-C_3N_4) is a robust and nontoxicity polymeric catalyst with good properties [11]. It was constructed by the polymerization method as a photocatalytic water splitting catalyst in 2009 [12]. Up to now, g-C_3N_4 has been widely developed as an emerging and prospective catalyst in different areas, for example photocatalytic degradation of pollution [13], hydrogen evolution through photocatalytic water splitting [14] and CO_2 reduction [15]. Nowadays g-C_3N_4 with various morphologies have emerged,

such as quantum dots [16,17], nanotubes [18,19], bulk g-C_3N_4 and g-C_3N_4 nanosheets [20]. Two-dimensional g-C_3N_4 nanosheets have been intensively explored because of their outstanding photocatalytic performance in the past few years [20]. For example, the hydrogen generation ability of two-dimensional g-C_3N_4 nanosheets was improved by Lu and co-workers [21]. It is reported that g-C_3N_4 nanosheets have an improved catalytic performance compared with bulk g-C_3N_4, benefiting from its enlarged redox potentials [22], and prolonged charge carrier lifetime. As has been reported, a short transfer path can be obtained in the g-C_3N_4 nanosheets [22]. Therefore, efficient performance of g-C_3N_4 with 2D ultra-thin structure can be anticipated. In 2015, Liu and co-workers reported that the as-synthesized g-C_3N_4 nanosheets possessed an efficient water splitting ability by nature-inspired environment "phosphorylation" [23]. Unfortunately, g-C_3N_4 has a lot of defects, such as an inner self-combination of electrons and holes, limited light response ability, and so on [24]. To overcome the above shortcomings and greatly enhance its photocatalytic H_2 production activity, semiconductor composite [25], dye sensitization, and co-catalyst modification [26] have been tried.

Among the semiconductor composites, the Z-scheme charge transfer pathway is a practical strategy. Its prominent advantages are the efficient separation of e^- and h^+ at conduction band edges (E_{CB}) of one semiconductor and valence band edges (E_{VB}) of other semiconductors, respectively. Therefore, it can inhibit the inner self-combination of electrons and holes. The transfer process schematic diagram has the same shape as the letter Z, called the Z charge transfer pathway. What is more, it is extensively utilized by researchers to boost the effective separation and migration of charges, facilitate hydrogen generation of water splitting and perform a superior photocatalytic performance. For instance, Xie and co-workers synthesized Ag-AgI/BiOI-Bi_2O_3 photocatalyst with Z-scheme multi-charge transfer pathway, which exhibited excellent photocatalytic performance [27]. Qu et al. constructed Ag_2MoO_4/Ag/AgBr Z-scheme composites. The obtained composites exhibited an excellent performance for RhB photocatalytic degradation under various reaction conditions [28]. The photocatalysts with Z-scheme photocatalytic charge transfer pathway have different band structures. The p-type transition metal oxide semiconductor, Co_3O_4, is a narrow band gap photocatalyst, and has been widely employed as an excellent catalyst [29]. Co_3O_4 and g-C_3N_4 can meet the requirements of Z-scheme charge transfer pathway due to their suitable valence band edges and conduction band edges [30]. Through the modification of Co_3O_4 and construction of Z-scheme charge transfer pathway, an electric field between Co_3O_4 and g-C_3N_4 photocatalysts is constructed, which is of benefit to the charge separation and migration. Therefore, improved photocatalytic performance can be obtained on Co_3O_4/g-C_3N_4.

Co_3O_4/g-C_3N_4 catalysts have been applied to degrade tetracycline [30], several dye pollutants [31] and photocatalytic water oxidation [32]. They all exhibited outstanding photocatalytic performances. For instance, Jin et al. synthesized Co_3O_4/g-C_3N_4 as peroxymonsulfate-mediated photocatalytic catalysts, which showed good activity for tetracycline degradation [30]. Qu et al. synthesized Co_3O_4/g-C_3N_4 composites with outstanding photocatalytic peroxymonosulfate activation performance for dyes' degradation [31].

As has been reported, introducing co-catalysts can greatly improve the hydrogen evolution reaction performance of semiconductors. Researchers have found that modification with noble metal Pt can boost the photocatalysts' water splitting activity [33,34]. As an electron mediator, Pt has a low Fermi level, which has an important impact on the H_2 evolution performance.

Based on former reports, g-C_3N_4 nanosheets with uniform thickness were synthesized by a polymerization method in the paper. Co_3O_4 was then introduced via an electrostatic interaction–calcination method to form Z-scheme charge transfer pathway in order to obtain efficient separation of charge carriers and high photocatalytic water splitting performance. With further Pt modification, better activity was obtained. The Z-scheme photocatalytic charge transfer pathway of Co_3O_4/g-C_3N_4 was put forward based on the experimental data.

2. Materials and Methods

2.1. Materials

All the reagents that were used were analytical pure. Triethanolamine (TEOA) was purchased from Aladdin Industry Corporation, Shanghai, China. Melamine was purchased from Tianjin Jiangtian Chemical Technology Co. Ltd., Tianjin, China. Ammonia chloride was purchased from Wind Ship Chemical Reagent Technology Co. Ltd., Tianjin, China. Anhydrous ethanol and ammonium bicarbonate were purchased from Guangfu Technology Development Co. Ltd., Tianjin, China. Cobalt chloride hexahydrate and chloroplatinic acid were purchased from Masco Chemical Co. Ltd., Tianjin, China.

2.2. Fabrication of g-C_3N_4

The large-scale production of few-layer and ultra-thin g-C_3N_4 nanosheets with uniform thickness was performed by the facile method of polymerization. 5 g melamine and 10 g ammonia chloride were fully grinded into powder and then calcinated at 550 °C for 4 h in the air atmosphere. This product was collected and named as g-C_3N_4.

2.3. Synthesis of the Ultra-Thin Co_3O_4/g-C_3N_4 Catalysts

The series Co_3O_4/g-C_3N_4 nanosheets were prepared via electrostatic interaction and calcination methods. 0.72 g g-C_3N_4 was sonicated for 0.5 h to disperse in 100 mL anhydrous ethanol. Subsequently, different masses of $CoCl_2 \cdot 6H_2O$ were added into the above system, followed with a stoichiometric ratio of NH_4HCO_3, and n($CoCl_2 \cdot 6H_2O$): n(NH_4HCO_3) = 1:3 [31]. After continuous stirring for 6 h, the sample was centrifugated, washed and dried at 85 °C. The as-synthesized materials were calcinated at 350 °C for 2 h. The series Co_3O_4/g-C_3N_4 catalysts with various mass ratios were collected, and are denoted as 0.3, 0.5, 1, 3, 6, 12 wt.% Co_3O_4/g-C_3N_4, respectively.

For comparison, the pure Co_3O_4 was fabricated by calcination of $CoCl_2 \cdot 6H_2O$ at 600 °C for 4 h.

2.4. Characterization

The X-ray powder diffraction (XRD) was characterized by a diffractometer from Rigaku Corporation. Scanning electron microscopy image was observed by a SU3500 (Hitachi, Tokyo, Japan) microscope. Elemental analysis was explored by Elemental Analyzer (Vario EL cube, Langenselbold, Germany). The ICP analysis was performed by Inductive Coupled Plasma Emission Spectrometer (SpectroBlue, Kleve, Germany). Transmission electron microscopy (TEM) was observed by a FEI TalosF200X instrument. EDS analyses were characterized by an energy dispersive X-ray spectroscope (Bruker, Billerica, MA, USA). Atomic force microscopy (AFM) images were performed by the Bruker icon AFM instrument. The X-ray photoelectron spectroscopy (XPS, Thermo escalab 250Xi) analysis was characterized on a photoemission spectroscopy, using a mono AlKα radiation source. The UV–Vis diffuse reflection spectra (UV–Vis DRS) was explored by a UV–Vis spectrophotometer (UV3600-Plus, Shimadzu, Kyoto, Japan). Photoluminescence spectra (PL) was conducted by a spectrophotometer (PTI, New York, NY, USA). Electrochemical experiments were explored with a workstation (Zahner Zenium, Kronach, Germany).

2.5. Photocatalytic Activity

The H_2 production tests were implemented with the catalyst (50 mg), which was dispersed in triethanolamine solution (10% vol TEOA) in the Labsolar-6A online system. 0.5 wt.% Pt, which was used as co-catalyst, was in-situ reduced by light on the catalysts by adding H_2PtCl_6 aqueous solution in the above suspension of the reaction. After vacuuming, the Argon gas was added. A 300 W Xenon lamp was served to achieve the system irradiation during tests. The solution temperature was controlled at 5 °C to avoid the thermal effect produced by light. Additionally, the tests were carried out using a gas chromatograph and the carrier gas is Argon (GC D7900 II, Tianmei, Shanghai, China).

3. Results and Discussion

3.1. XRD Analysis

The XRD measurement was characterized to confirm the phase of the catalysts, as shown in Figure 1. The peaks at 2θ = 13. 0 and 27.7° were indexed to the characteristic peaks of g-C_3N_4 [5,35]. The diffraction peaks at 2θ = 19.0°, 31.3°, 36.9°, 38.5°, 44.8°, 55.7°, 59.4° and 65.2° were indexed as (1 1 1), (2 2 0), (3 1 1), (2 2 2), (4 0 0), (4 2 2), (5 1 1) and (4 4 0) plane of cubic Co_3O_4 (PDF#42-1467), respectively. It was evident that the peaks of Co_3O_4 and g-C_3N_4 were both existed in the 6% and 12% Co_3O_4/g-C_3N_4 photocatalysts' XRD patterns. No obvious Co_3O_4 peaks were observed in Co_3O_4/g-C_3N_4 samples with 0.3%, 0.5%, 1% and 3% Co_3O_4. That might be owing to the relatively low content and high distribution of Co_3O_4 [36]. What is more, as clearly demonstrated, the peaks of the photocatalysts were sharp and strong, illustrating that the samples possessed an excellent crystallization. There were no peaks of other phases in Figure 1, which indicated the good purity of the synthesized photocatalysts.

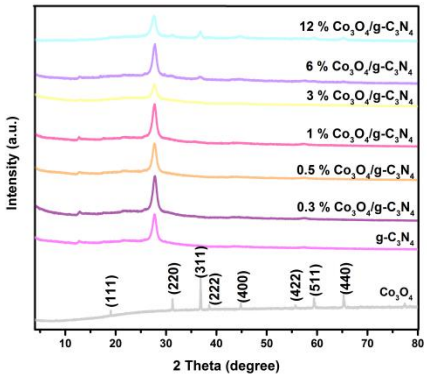

Figure 1. XRD pattern of fabricated samples.

3.2. EA and ICP

For the g-C_3N_4 sample, the atomic ratio of C element and N element was investigated by EA. The value exhibited a result that the atomic ratio of C/N = 3.00: 4.27, which was very close to the value of g-C_3N_4. Based on XRD analysis results, the as-synthesized products were pure g-C_3N_4.

The amounts of Co element in the as-prepared catalysts were monitored by the ICP. The actual contents of 0.3%, 0.5%, 1%, 3%, 6% and 12% Co_3O_4/g-C_3N_4 is 0.3540, 0.5354, 1.146, 3.038, 6.253, 12.44 wt.%, respectively. The corresponding contents of Co_3O_4 in the series Co_3O_4/g-C_3N_4 photocatalysts are close to theoretical values. Due to the negative zeta potentials of g-C_3N_4, there was strong electrostatic interaction between Co^{2+} and g-C_3N_4 nanosheets [37]. As a result, the added Co^{2+} should have no considerable loss. Actually, the actual weight ratio of Co_3O_4 to g-C_3N_4 in the prepared Co_3O_4/g-C_3N_4 catalysts was a little higher than original $CoCl_2 \cdot 6H_2O$ to g-C_3N_4. It was assignable to the slight weight loss after the second calcination process of g-C_3N_4.

3.3. Morphology Analysis

The microstructure of as-fabricated catalysts was presented in Figure 2. From Figure 2a, Co_3O_4 had polyhedral structure, and the 0.5% Co_3O_4/g-C_3N_4 showed an irregular and crinkly structure. Pt/0.5% Co_3O_4/g-C_3N_4 exhibited 2D morphology with a crinkly nanosheet structure, which seem to be a loose and soft product with a diameter of several micrometers. As observed in the images, the microstructures of 0.5% Co_3O_4/g-C_3N_4 and Pt/0.5% Co_3O_4/g-C_3N_4 were nanosheets. The composition and elements distribution of 0.5% Co_3O_4/g-C_3N_4 and Pt/0.5% Co_3O_4/g-C_3N_4 were further investigated by EDS maps, as displayed in Figures 3 and 4. All of the elements were uniformly dispersed in the photcatalysts, and no signals of other elements were observed. Furthermore, the existence of C, N,

Co, O and Pt were highly coincided with the area of g-C_3N_4. It seems that Co_3O_4 and Pt could be uniformly deposited on the g-C_3N_4.

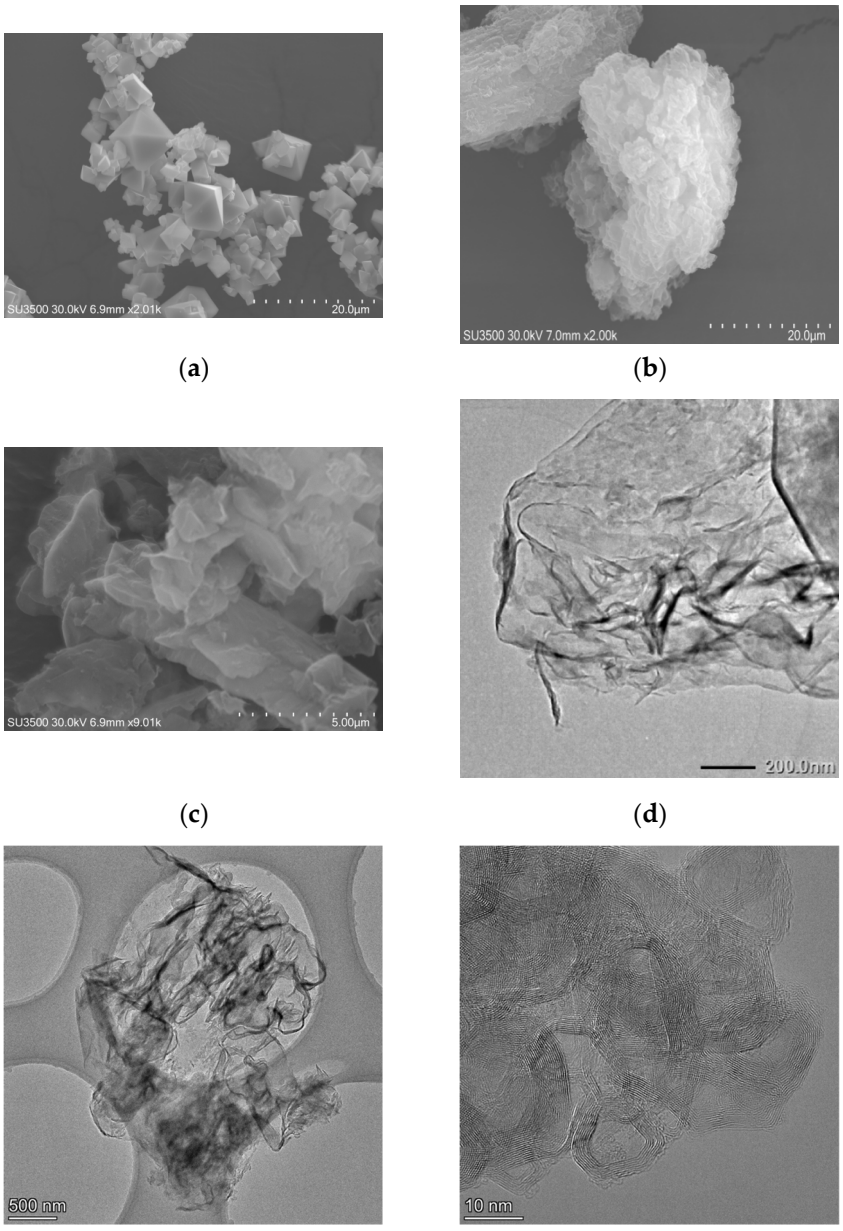

Figure 2. SEM images of (**a**) Co_3O_4, (**b**) 0.5% Co_3O_4/g-C_3N_4, and (**c**) Pt/0.5% Co_3O_4/g-C_3N_4. The TEM image of (**d**) 0.5% Co_3O_4/g-C_3N_4 and (**e**,**f**) Pt/0.5% Co_3O_4/g-C_3N_4.

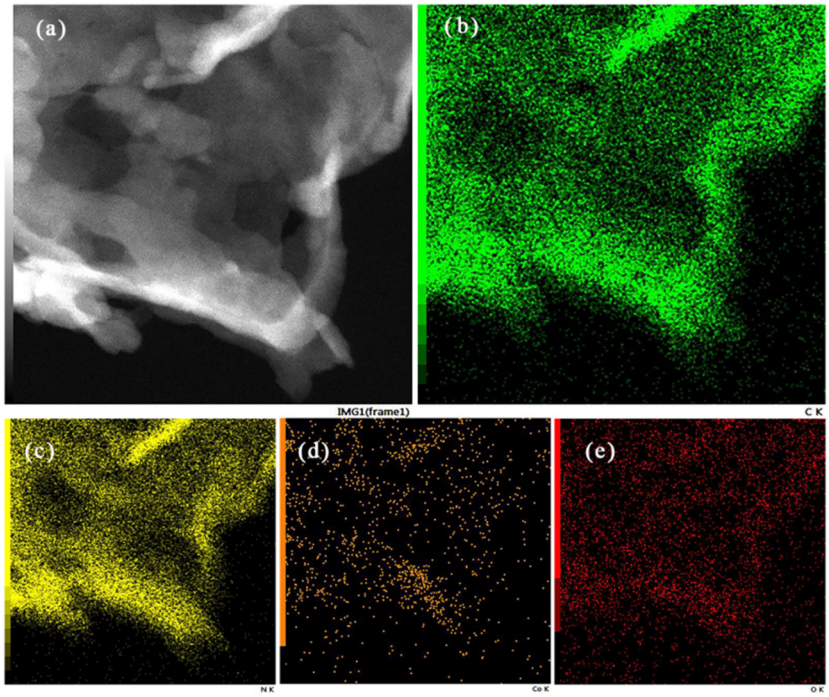

Figure 3. (**a**) The TEM image of 0.5% Co_3O_4/g-C_3N_4. (**b**–**e**) Elemental maps of the catalyst: (**b**) C, (**c**) N, (**d**) Co and O elements.

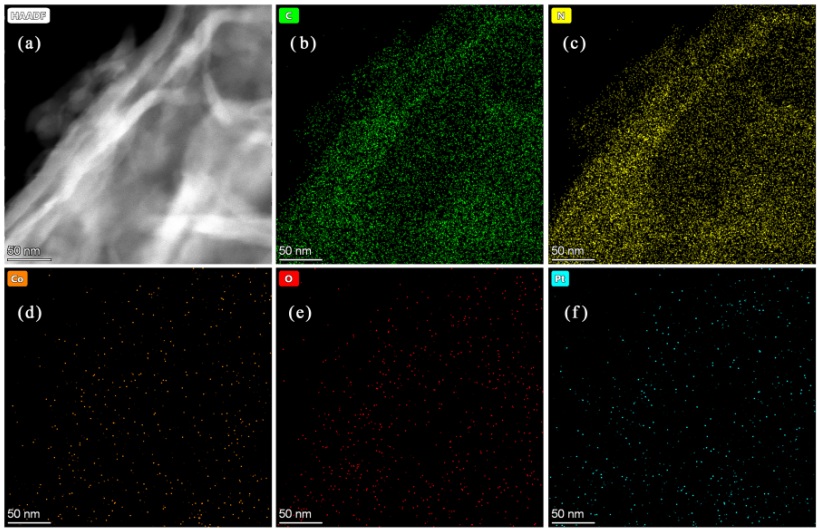

Figure 4. (**a**) HAADF-TEM image of Pt/0.5% Co_3O_4/g-C_3N_4. (**b**–**f**) Elemental maps of the catalyst: (**b**) C, (**c**) N, (**d**) Co, (**e**) O and (**f**) Pt elements.

3.4. AFM Analysis

To further investigate the structure and height profiles of the photocatalysts, AFM was performed. The images and corresponding thickness of samples were presented in Figure 5. The architectures of the g-C_3N_4 were 2D ultra-thin nanosheets, with 1–2 nm step height. As illustrated in Figure 5c,d, there is no obvious step height change for 0.5% Co_3O_4/g-C_3N_4 ultra-thin nanosheets. Additionally, g-C_3N_4 and 0.5% Co_3O_4/g-C_3N_4 nanosheets both exhibited few-layer ultra-thin nanosheets with uniform thickness. Ultrathin nanosheets had a short bulk diffusion length [22,38]. Compared with bulk g-C_3N_4, ultrathin g-C_3N_4 nanosheets and 0.5% Co_3O_4/g-C_3N_4 photocatalysts had a shorter electron transfer path, which can increase the lifetime of photoexcited electrons. The unique structure of few-layer g-C_3N_4 photocatalyst generated numerous charge transfer nanochannels and provided a

short transfer path for electron transfer, which would promote the efficient separation and migration of e^- and h^+ [22].

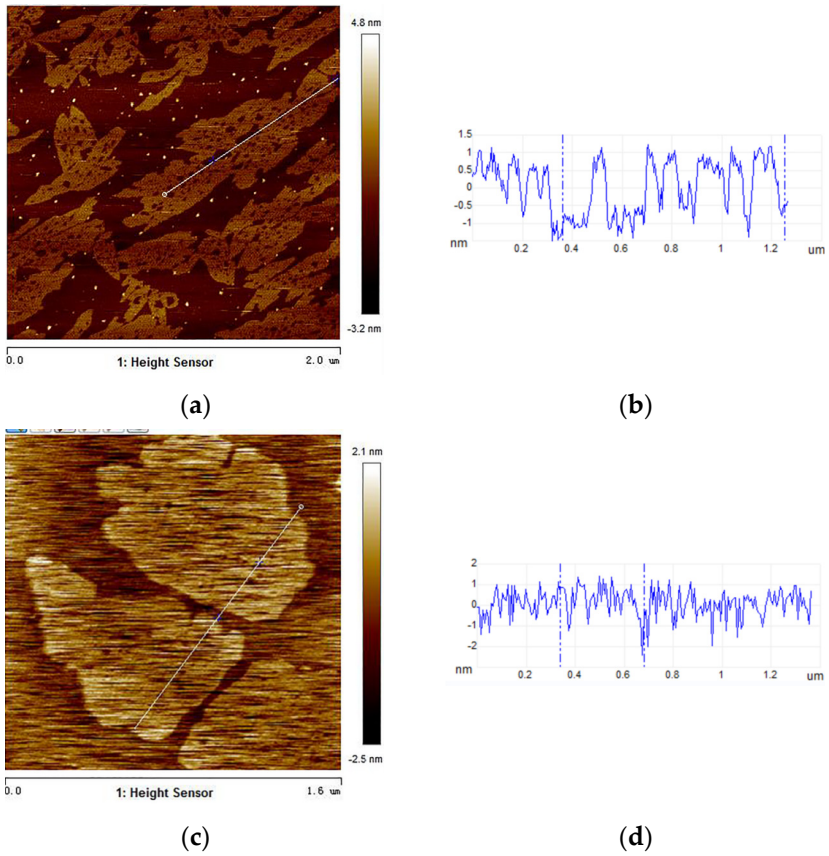

Figure 5. (**a**,**b**) AFM images and corresponding thickness of pure 2D g-C_3N_4 and (**c**,**d**) 0.5 % Co_3O_4/g-C_3N_4.

3.5. XPS Analysis

To confirm the element compositions and chemical states in the as-synthesized 0.5% Co_3O_4/g-C_3N_4, the XPS analysis was conducted. From XPS survey spectrum (Figure 6a), C 1s, N 1s and O 1s peaks were evident. What is more, no signals assigned to other elements were displayed in this survey spectrum, suggesting that the purity of the samples is very high. As displayed in Figure 6b, the peak at 287.7 eV is due to sp^2 C atoms, which can bond to N atoms in catalysts [39]. Additionally, the peak at 293.1 eV is owing to π-excitation [40]. Evidently, N 1s has three different peaks at 398.1 eV, 400.0 eV and 404.0 eV in Figure 5c assigning to sp^2 N atoms of triazine rings, bridging nitrogen atoms in $(N–(C)_3)$ and the charging effects of the hetero-cycles or positive charge localization [41], respectively. The Co 2p at the peaks of 780.4 and 796.1 eV are ascribed to Co $2p_{3/2}$ and Co $2p_{1/2}$, suggesting that Co_3O_4 exists in the photocatalysts [42,43]. Compared with g-C_3N_4, there was negative energy shift of C 1s and N 1s in 0.5% Co_3O_4/g-C_3N_4 photocatalysts, indicating that the e^- are transferred from Co_3O_4 to g-C_3N_4 [31]. As discussed in the Z-scheme charge transfer system, e^- on CB of Co_3O_4 can migrate to VB of the other semiconductor. Therefore, Z-scheme charge transfer pathway of Co_3O_4/g-C_3N_4 system agreed with the results of negative binding energy shift in 0.5% Co_3O_4/g-C_3N_4 photocatalysts. These results take firm evidence that the Co_3O_4 and g-C_3N_4 were co-existed in the samples and Z-scheme charge transfer pathway was constructed in photocatalysts.

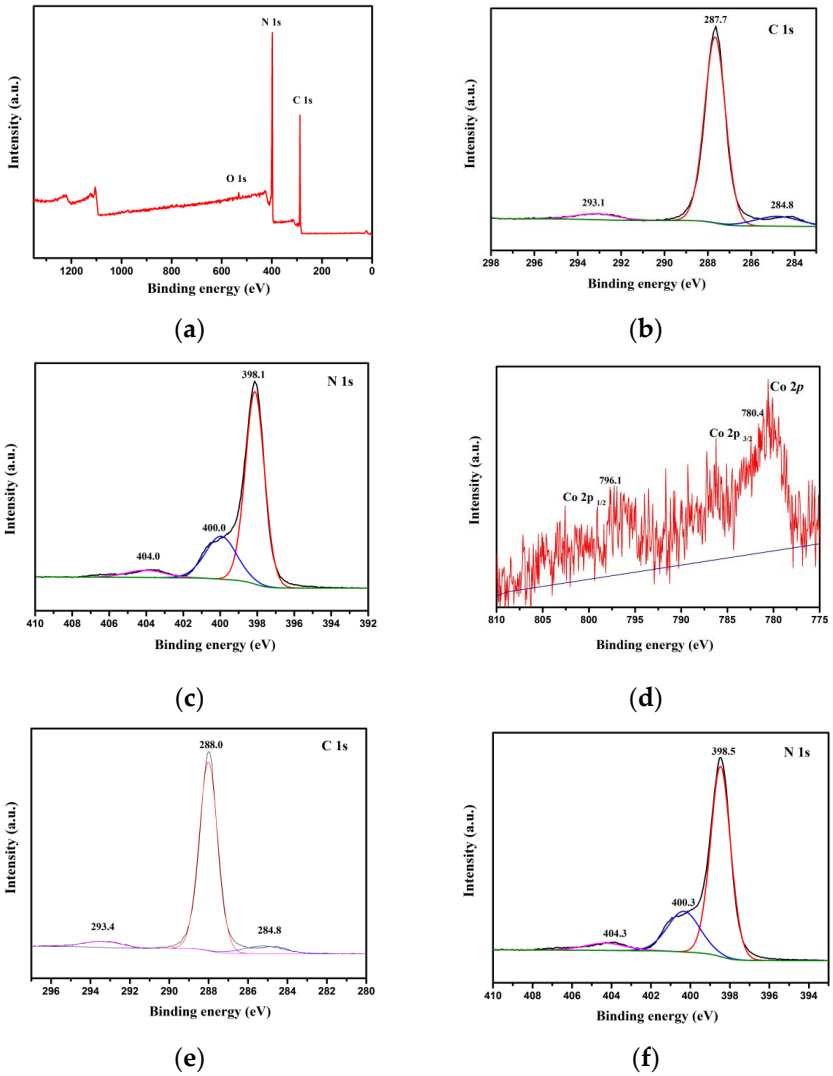

Figure 6. XPS spectra (**a**–**d**) survey, C 1s, N 1s and Co 2p of 0.5 % Co_3O_4/g-C_3N_4, (**e**,**f**) C 1s and N 1s of g-C_3N_4, respectively.

3.6. UV–Vis DRS Analysis

The UV–Vis DRS spectrophotometer analysis was performed to measure optical absorption properties of the catalysts. 0.5% Co_3O_4/g-C_3N_4 possessed a strong absorption and its edge located at 443 nm in Figure 6a. Additionally, although the absorption edges and bandgap energies of g-C_3N_4 and 0.5% Co_3O_4/g-C_3N_4 had no apparent distinction, optical absorption intensity of 0.5% Co_3O_4/g-C_3N_4 was apparently increased, which made it easier to harvest light. The spectra (Figure 7a) of the catalysts suggested that the samples displayed a strong absorption all between 200–440 nm, which covered ultraviolet and visible regions. These photocatalysts can respond to the visible light and their responsiveness was enhanced, which has probably a more important advantage to photocatalytic water splitting. Bandgaps of Co_3O_4, g-C_3N_4 and 0.5% Co_3O_4/g-C_3N_4 photocatalysts were achieved by the Tauc plots, and results are presented in Figure 7b. The bandgap (E_g) of catalysts can be received by the Tauc Equation [44]. Because the Co_3O_4 [45] and g-C_3N_4 [46] are typical direct semiconductors, n in the Tauc equation should be all 1/2. The E_g of as-prepared g-C_3N_4 and Co_3O_4 are 2.8 eV and 2.0 eV, respectively. The E_{CB} values of Co_3O_4 and g-C_3N_4 are obtained via this equation.

$$E_{CB} = \chi - E_e - 0.5E_g \quad (1)$$

χ for g-C_3N_4 and Co_3O_4 are 4.64 [47] and 5.90 [48], respectively. E_{CB} of g-C_3N_4 and Co_3O_4 are −1.26 eV and 0.4 eV, respectively. So E_{VB} values of g-C_3N_4 and Co_3O_4 are 1.54 eV and 2.4 eV, respectively. Because of the appropriate band structure of two semiconductors, the e^- would like to transfer from CB of Co_3O_4 to VB of g-C_3N_4. Finally, e^- and h^+ accumulate at CB of g-C_3N_4 and VB of Co_3O_4, respectively. Charge carriers can be effectively separated. These data of g-C_3N_4 and Co_3O_4 can be known based on the formulas and experiments.

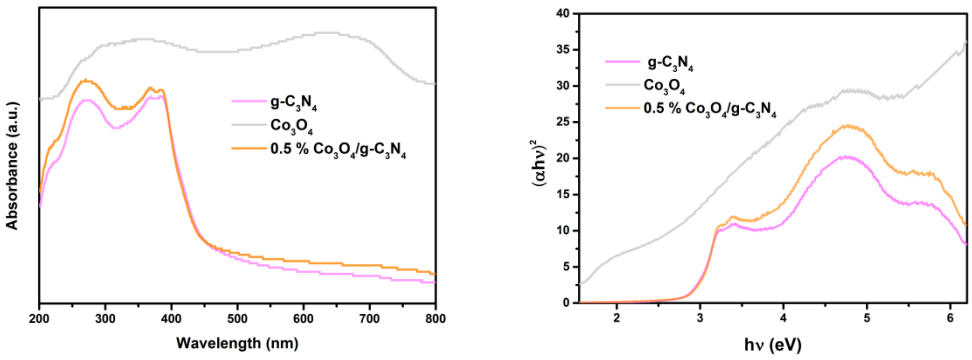

Figure 7. (**a**) UV–Vis DRS of the catalysts. (**b**) Bandgap energies of the photocatalysts.

3.7. PL

As displayed in Figure 8, the recombination ability of e^- and h^+ was speculated from the photoluminescence intensity of the samples. All the photocatalysts were evaluated at the excitation wavelength, which was 320 nm. Generally, the higher intensity of the PL emission spectra means a worse separation ability of carriers [49]. The spectrum of 0.5% Co_3O_4/g-C_3N_4 catalyst showed lower emission intensity than the intensity of g-C_3N_4, leading to a lower recombining frequency of e^- and h^+ in 0.5% Co_3O_4/g-C_3N_4. The lower the peak of photoluminescence spectra presented, the more excellent catalytic performance can be anticipated. It seems that 0.5% Co_3O_4/g-C_3N_4 catalyst may have a better photocatalytic performance than pure g-C_3N_4.

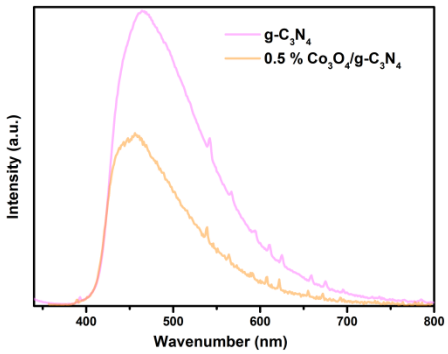

Figure 8. Steady-state photoluminescence spectra of fabricated photocatalysts.

3.8. Photoelectrochemical Analysis

The photocurrent measurement was produced under the irradiation of 429 nm wavelength light, as illustrated in Figure 9. The photocurrent immediately increased to a value and remained when the light irradiated on the catalysts. The photocurrent decreased as soon as the light turned off. It manifested that 0.5% Co_3O_4/g-C_3N_4 has a photocurrent response and the photocurrent value is around 10 nA at 0.1 V. However, no photocurrent existed in g-C_3N_4. It indicated that 0.5% Co_3O_4/g-C_3N_4 is visible to light-responsive photocatalysts. After Co_3O_4 was introduced, the g-C_3N_4 catalyst can respond to visible light, and a photocurrent was exhibited. That should be attributed to the formation of Z-scheme charge transfer pathway, which resulted in improved separation and migration

of the photo-induced charges. As a result, a photocurrent with higher intensity can be obtained.

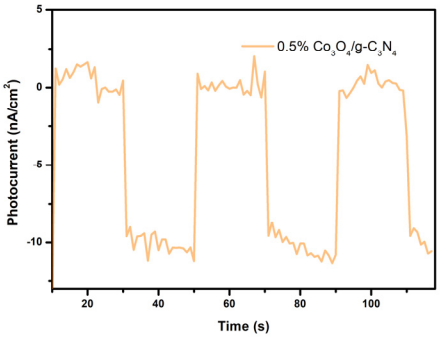

Figure 9. The photocurrent measurement spectra of the 0.5% Co_3O_4/g-C_3N_4 catalysts.

3.9. Photocatalytic Activity and Cycling Tests

As illustrated in Figure 10a, g-C_3N_4 exhibits no activity. However, the series Co_3O_4/g-C_3N_4 catalysts all present good photocatalytic performance, and 0.5% Co_3O_4/g-C_3N_4 has the fine H_2 evolution rate of 8.774 μmol·g^{-1}·h^{-1}. Obviously, the modification of Co_3O_4 can greatly promote the water splitting reaction rate of g-C_3N_4. The results of photocatalytic activity tests can be proved by photoelectrochemical analysis. As indicated in the photoelectrochemical analysis, the g-C_3N_4 can respond to 429 nm only after Co_3O_4 was modified. Therefore, the quantum yield of g-C_3N_4 is low. Catalytic activity of g-C_3N_4 is also low. The photoluminescence spectra analysis showed that e^- and h^+ in the g-C_3N_4 have higher recombination rates. It suggested that g-C_3N_4 has a lower photocatalytic hydrogen production.

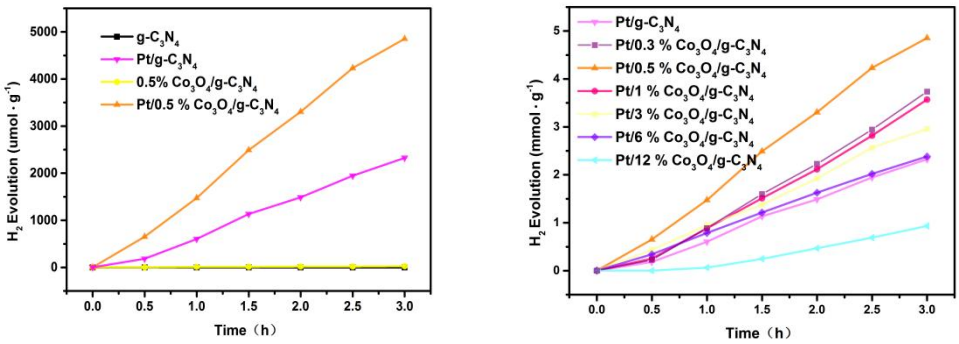

(**a**) (**b**)

Figure 10. (**a**,**b**) Photocatalytic hydrogen evolution performance of prepared catalysts.

According to the band structure of Co_3O_4 and g-C_3N_4 as we noted above, the reasonable photocatalytic charge transfer pathway was preliminarily put forward to explain the reason for catalytic improved-performance of 0.5% Co_3O_4/g-C_3N_4 in Figure 11. The electrons of Co_3O_4 and g-C_3N_4 are photo-generated from VB to CB in response to irradiation. After calcination, interaction between Co_3O_4 and g-C_3N_4 was enhanced. The e^- on CB of Co_3O_4 would quickly migrate to VB of g-C_3N_4 and combine with h^+, which replaced inner self-combination. Some holes were reacted with TEOA, which worked as an oxidation sacrificial agent. Therefore, the electric field between Co_3O_4 and g-C_3N_4 was formed, with electrons and holes accelerated at different parts. The electric field can promote the directional transfer of charges and introduction of Co_3O_4 can boost the electric field of Co_3O_4/g-C_3N_4. Hence, the existence of Co_3O_4 effectively promoted the interfacial charges to separate and transfer and the hydrogen generation, leading to superior photocatalytic performance. What is more, the XPS analysis indicated that e^- are transferred from Co_3O_4

to g-C_3N_4 nanosheets. It suggested that the Z-scheme charge transfer pathway was in agreement with experiment results.

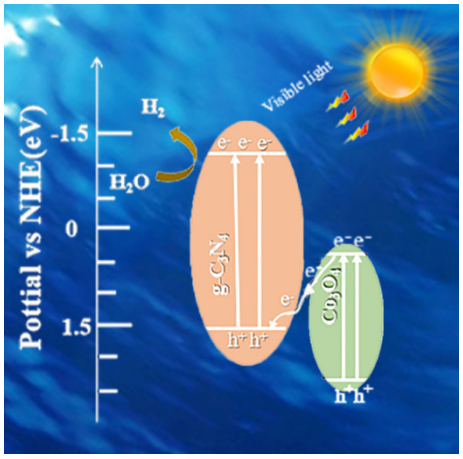

Figure 11. Proposed mechanism of photocatalytic system.

The probable reactions process of photocatalytic hydrogen generation is as follows:

$$Co_3O_4/g\text{-}C_3N_4 + hv \rightarrow Co_3O_4(e^- + h^+)/g\text{-}C_3N_4(e^- + h^+) \quad (2)$$

$$h^+_{VB}(Co_3O_4) + TEOA \rightarrow \text{oxidation product of sacrificial reagent} \quad (3)$$

$$e^-_{CB}(g\text{-}C_3N_4) + 2H_2O \rightarrow H_2 + 2OH^- \quad (4)$$

Thence, the proposed Z-scheme charge transfer pathway of photocatalysts showed good separation and migration of e^- and h^+. The obvious enhancement of the hydrogen generation ability of the 0.5% Co_3O_4/g-C_3N_4 ultra-thin nanosheets may attribute to the significant and ideal Z-scheme photocatalytic charge transfer pathway.

After Pt was added, further efforts were made to improve the performance of Co_3O_4/g-C_3N_4. As presented in Figure 10a, Pt/0.5% Co_3O_4/g-C_3N_4 exhibited a predominant rate and the average rate was up to 1620 μmol·g^{-1}·h^{-1}. This is 2.1 times the photocatalytic performance of Pt/g-C_3N_4.

To explore the influence of Co_3O_4 contents on the performance of the Pt/Co_3O_4/g-C_3N_4, results of Pt/Co_3O_4/g-C_3N_4 with different Co_3O_4 contents were shown in Figure 10b. From this figure, it can be observed that all photocatalysts manifested improved hydrogen generation activity compared with Pt/g-C_3N_4, except Pt/12% Co_3O_4/g-C_3N_4. Owning to the relatively low content of Co_3O_4 (0.5 % Co_3O_4), Pt was mainly deposited on g-C_3N_4 nanosheets. When the catalyst was illuminated, the electrons migrated from Co_3O_4 to g-C_3N_4, and were finally transferred to Pt. The H^+ in the solution obtained the electrons from the Pt particles to form H_2. When the Co_3O_4 content was relatively low (0.3%), Z-scheme charge transfer pathway is still the main pathway in this photocatalytic system. However, the amount of electrons and holes in Co_3O_4 was relatively low than that in the 0.5% one. Therefore relatively large amounts of holes in g-C_3N_4 were reacted with TEOA instead of combining with the electrons in Co_3O_4. As a result, e^- and h^+ in the Pt/0.3% Co_3O_4/g-C_3N_4 have higher recombination rates than in Pt/0.5% Co_3O_4/g-C_3N_4, and the Pt/0.3% Co_3O_4/g-C_3N_4 exhibited lower photoactivity. When Co_3O_4 contents increased, Co_3O_4 will accumulate. More and more Pt/Co_3O_4 interfaces formed, and the electrons migrated from Co_3O_4 to Pt, instead of combining with the holes in g-C_3N_4. Consequently, the Z-scheme charge transfer pathway was blocked, and the activity of Co_3O_4/g-C_3N_4 decreased with the increasing Co_3O_4 contents.

Cycling stability tests of the optimal Pt/0.5% Co_3O_4/g-C_3N_4 were evaluated by a recycle experiment, which was presented in Figure 12. It could suggest that after four successive cycles, no noticeable diminution was observed within 20 h with TEOA as sacrificing

agents, suggesting that the Pt/0.5% Co_3O_4/g-C_3N_4 photocatalyst had an excellent stability and it is reusable for practical applications.

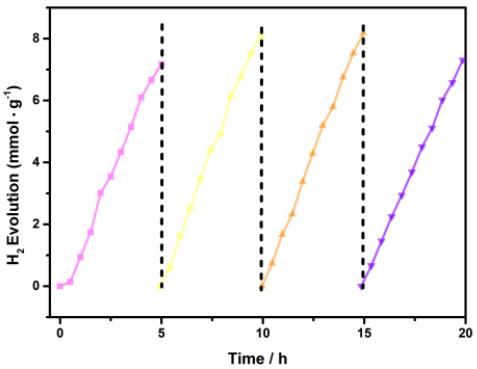

Figure 12. Photocatalytic stability performance of Pt/0.5% Co_3O_4/g-C_3N_4.

4. Conclusions

In this paper, g-C_3N_4 ultra-thin nanosheets were fabricated via the polymerization method. The Co_3O_4/g-C_3N_4 series were fabricated by an electrostatic interaction-calcination treatment. The various characterization results indicated that the Co_3O_4/g-C_3N_4 catalysts exhibit Z-scheme charge transfer pathway, and possessed excellent photocatalytic hydrogen evolution performance with high stability and fine charge transfer ability. After Pt is added, the Co_3O_4/g-C_3N_4 exhibited better activity, and Pt/0.5% Co_3O_4/g-C_3N_4 exhibited the best activity, with a hydrogen generation rate of 1620 $\mu mol \cdot g^{-1} \cdot h^{-1}$. Based on the characterization and environment data, the catalytic reaction charge transfer pathway of Pt/Co_3O_4/g-C_3N_4 was proposed. Therefore, the work provided a promising method to design efficient and reusable photocatalytic systems with Z-scheme charge transfer pathways for solar-energy conversion. Further practical applications of this Z-scheme charge transfer pathway were anticipated.

Author Contributions: Conceptualization and methodology, Y.G. and W.L.; software, Y.G.; validation, Y.G., W.D. and G.Z.; formal analysis, Y.G., W.L. and W.D.; investigation, Y.G. and W.D.; resources, Y.G.; data curation, Y.G., W.D. and S.W.; writing—original draft preparation, Y.G.; writing—review and editing, Y.G. and W.L.; visualization, Y.G., W.D. and L.J.; supervision, B.Z., W.H. and S.Z.; project administration, B.Z., W.H. and S.Z.; funding acquisition, B.Z., W.H. and S.Z. All authors have read and agreed to the published version of the manuscript.

Funding: This research was funded by the National Natural Science Foundation of China, grant number 21271110.

Data Availability Statement: The data presented in this study are available on request from the corresponding author.

Conflicts of Interest: The authors declare no conflict of interest.

References

1. Huang, Z.F.; Song, J.; Wang, X.; Pan, L.; Li, K.; Zhang, X.W.; Wang, L.; Zou, J.J. Switching charge transfer of $C_3N_4/W_{18}O_{49}$ from type-II to Z-scheme by interfacial band bending for highly efficient photocatalytic hydrogen evolution. *Nano Energy* **2017**, *40*, 308–316. [CrossRef]
2. Wang, Q.; Hisatomi, T.; Jia, Q.; Tokudome, H.; Zhong, M.; Wang, C.Z.; Pan, Z.H.; Takata, T.; Nakabayashi, M.; Shibata, N.; et al. Scalable water splitting on particulate photocatalyst sheets with a solar-to-hydrogen energy conversion efficiency exceeding 1%. *Nat. Mater.* **2016**, *15*, 611–615. [CrossRef]
3. Tan, M.; Yu, C.; Li, J.; Li, Y.; Tao, C.D.; Liu, C.B.; Meng, H.M.; Su, Y.J.; Qiao, L.J.; Bai, Y. Engineering of g-C_3N_4-based photocatalysts to enhance hydrogen evolution. *Adv. Colloid Interface Sci.* **2021**, *295*, 102488. [CrossRef] [PubMed]
4. Wang, M.; Xi, X.; Gong, C.; Zhang, X.L.; Fan, G.L. Open porous $BiVO_4$ nanomaterials: Electronspinning fabrication and enhanced visible light photocatalytic activity. *Mater. Res. Bull.* **2016**, *74*, 258–264. [CrossRef]
5. Su, T.; Hood, Z.D.; Naguib, M.; Bai, L.; Luo, S.; Rouleau, C.M.; Ivanov, I.N.; Ji, H.B.; Qin, Z.Z.; Wu, Z.L. 2D/2D heterojunction of Ti_3C_2/g-C_3N_4 nanosheets for enhanced photocatalytic hydrogen evolution. *Nanoscale* **2019**, *11*, 8138–8149. [CrossRef] [PubMed]

6. Cao, S.; Piao, L.; Chen, X. Emerging photocatalysts for hydrogen evolution. *Trends Chem.* **2020**, *2*, 57–70. [CrossRef]
7. Qin, Y.; Li, H.; Lu, J.; Meng, F.Y.; Ma, C.C.; Yan, Y.S.; Meng, M.J. Nitrogen-doped hydrogenated TiO_2 modified with CdS nanorods with enhanced optical absorption, charge separation and photocatalytic hydrogen evolution. *Chem. Eng. J.* **2020**, *384*, 123275. [CrossRef]
8. Chen, J.; Shen, Z.; Lv, S.; Shen, K.; Wu, R.F.; Jiang, X.F.; Fan, T.; Chen, J.Y.; Li, Y.W. Fabricating sandwich-shelled ZnCdS/ZnO/ZnCdS dodecahedral cages with "one stone" as Z-scheme photocatalysts for highly efficient hydrogen production. *J. Mater. Chem. A* **2018**, *6*, 19631–19642. [CrossRef]
9. Zhou, H.; Qu, Y.; Zeid, T.; Duan, X.F. Towards highly efficient photocatalysts using semiconductor nanoarchitectures. *Energy Environ. Sci.* **2012**, *5*, 6732–6743. [CrossRef]
10. Wang, Q.; Domen, K. Particulate photocatalysts for light-driven water splitting: Mechanisms, challenges, and design strategies. *Chem. Rev.* **2019**, *120*, 919–985. [CrossRef]
11. Zhang, C.; Li, Y.; Shuai, D.; Shen, Y.; Xiong, W.; Wang, L.Q. Graphitic carbon nitride (g-C_3N_4)-based photocatalysts for water disinfection and microbial control: A review. *Chemosphere* **2019**, *214*, 462–479. [CrossRef]
12. Wang, X.; Maeda, K.; Thomas, A.; Takanabe, K.; Xin, G.; Carlsson, J.M.; Domen, K.; Antonietti, M. A metal-free polymeric photocatalyst for hydrogen production from water under visible light. *Nat. Mater.* **2009**, *8*, 76–80. [CrossRef]
13. Zhang, J.Y.; Zhang, S.H.; Li, J.; Zheng, X.C.; Guan, X.X. Constructing of 3D graphene aerogel-g-C_3N_4 metal-free heterojunctions with superior purification efficiency for organic dyes. *J. Mol. Liq.* **2020**, *310*, 113242. [CrossRef]
14. Wu, Z.; Liang, Y.; Yuan, X.; Zou, D.S.; Fang, J.; Jiang, L.B.; Zhang, J.; Yang, H.L.; Xiao, Z.H. MXene Ti_3C_2 derived Z–scheme photocatalyst of graphene layers anchored TiO_2/g-C_3N_4 for visible light photocatalytic degradation of refractory organic pollutants. *Chem. Eng. J.* **2020**, *394*, 124921. [CrossRef]
15. Wang, K.; Li, Q.; Liu, B.; Cheng, B.; Ho, W.K.; Yu, J.G. Sulfur-doped g-C_3N_4 with enhanced photocatalytic CO_2-reduction performance. *Appl. Catal. B Environ.* **2015**, *176*, 44–52. [CrossRef]
16. Nasir, M.S.; Yang, G.; Ayub, I.; Wang, S.L.; Yan, W. Tin diselinide a stable co-catalyst coupled with branched TiO_2 fiber and g-C_3N_4 quantum dots for photocatalytic hydrogen evolution. *Appl. Catal. B Environ.* **2020**, *270*, 118900. [CrossRef]
17. Chen, X.; Liu, Q.; Wu, Q.; Du, P.W.; Zhu, J.; Dai, S.Y.; Yang, S.F. Incorporating graphitic carbon nitride (g-C_3N_4) quantum dots into bulk-heterojunction polymer solar cells leads to efficiency enhancement. *Adv. Funct. Mater.* **2016**, *26*, 1719–1728. [CrossRef]
18. Mo, Z.; Zhu, X.; Jiang, Z.; Song, Y.H.; Liu, D.B.; Li, H.P.; Yang, X.F.; She, Y.B.; Lei, Y.C.; Yuan, S.Q.; et al. Porous nitrogen-rich g-C_3N_4 nanotubes for efficient photocatalytic CO_2 reduction. *Appl. Catal. B Environ.* **2019**, *256*, 117854. [CrossRef]
19. Liu, G.; Liao, M.; Zhang, Z.; Wang, H.Y.; Chen, D.H.; Feng, Y.J. Enhanced photodegradation performance of Rhodamine B with g-C_3N_4 modified by carbon nanotubes. *Sep. Purif. Technol.* **2020**, *244*, 116618. [CrossRef]
20. Tonda, S.; Kumar, S.; Kandula, S.; Shanker, V. Fe-doped and-mediated graphitic carbon nitride nanosheets for enhanced photocatalytic performance under natural sunlight. *J. Mater. Chem. A* **2014**, *2*, 6772–6780. [CrossRef]
21. Lu, X.; Xu, K.; Chen, P.; Jia, K.C.; Liu, S.; Wu, C.Z. Facile one step method realizing scalable production of g-C_3N_4 nanosheets and study of their photocatalytic H_2 evolution activity. *J. Mater. Chem. A* **2014**, *2*, 18924–18928. [CrossRef]
22. Meng, N.; Ren, J.; Liu, Y.; Huang, Y.; Petit, T.; Zhang, B. Engineering oxygen-containing and amino groups into two-dimensional atomically-thin porous polymeric carbon nitrogen for enhanced photocatalytic hydrogen production. *Energy Environ. Sci.* **2018**, *11*, 566–571. [CrossRef]
23. Liu, G.; Wang, T.; Zhang, H.; Meng, X.G.; Hao, D.; Chang, K.; Li, P.; Kako, T.; Ye, J.H. Nature-inspired environmental "phosphorylation" boosts photocatalytic H_2 production over carbon nitride nanosheets under visible-light irradiation. *Angew. Chem.* **2015**, *127*, 13765–13769. [CrossRef]
24. Wu, M.; He, X.; Jing, B.; Wang, T.; Wang, C.Y.; Qin, Y.L.; Ao, Z.M.; Wang, S.B.; An, T.C. Novel carbon and defects co-modified g-C_3N_4 for highly efficient photocatalytic degradation of bisphenol A under visible light. *J. Hazard. Mater.* **2020**, *384*, 121323. [CrossRef] [PubMed]
25. He, F.; Chen, G.; Yu, Y.; Hao, S.; Zhou, Y.S.; Zheng, Y. Facile approach to synthesize g-PAN/g-C_3N_4 composites with enhanced photocatalytic H_2 evolution activity. *ACS Appl. Mater. Interfaces* **2014**, *6*, 7171–7179. [CrossRef] [PubMed]
26. Dong, H.; Xiao, M.; Yu, S.; Wu, H.H.; Wang, Y.; Sun, J.X.; Chen, G.; Li, C.M. Insight into the Activity and Stability of Rh_xP Nano-Species Supported on g-C_3N_4 for Photocatalytic H_2 Production. *ACS Catal.* **2019**, *10*, 458–462. [CrossRef]
27. Yan, Q.; Xie, X.; Liu, Y.; Wang, S.B.; Zhang, M.H.; Chen, Y.Y.; Si, Y.S. Constructing a new Z-scheme multi-heterojunction photocataslyts Ag-AgI/BiOI-Bi_2O_3 with enhanced photocatalytic activity. *J. Hazard. Mater.* **2019**, *371*, 304–315. [CrossRef]
28. Qu, J.; Wang, X.; Zhang, Y.; Yuan, G.L. Multifunctional Ag nanoparticles in heterostructured Ag_2MoO_4/Ag/AgBr cubes with boosted photocatalytic performances. *Sol. Energy* **2018**, *170*, 124–131. [CrossRef]
29. Li, J.; Li, M.; Gui, P.; Zheng, L.N.; Liang, J.S.; Xue, G. Hydrothermal synthesis of sandwich interspersed $LaCO_3OH$/Co_3O_4/graphene oxide composite and the enhanced catalytic performance for methane combustion. *Catal. Today* **2019**, *327*, 134–142. [CrossRef]
30. Jin, C.; Wang, M.; Li, Z.; Kang, J.; Zhao, Y.; Han, J.; Wu, Z.M. Two dimensional Co_3O_4/g-C_3N_4 Z-scheme heterojunction: Mechanism insight into enhanced peroxymonosulfate-mediated visible light photocatalytic performance. *Chem. Eng. J.* **2020**, *398*, 125569. [CrossRef]
31. Gao, H.; Yang, H.; Xu, J.; Zhang, S.W.; Li, J.X. Strongly coupled g-C_3N_4 nanosheets-Co_3O_4 quantum dots as 2D/0D heterostructure composite for peroxymonosulfate activation. *Small* **2018**, *14*, 1801353. [CrossRef] [PubMed]

32. Zhang, J.; Grzelczak, M.; Hou, Y.; Maeda, K.; Domen, K.; Fu, X.Z.; Antonietti, M.; Wang, X.C. Photocatalytic oxidation of water by polymeric carbon nitride nanohybrids made of sustainable elements. *Chem. Sci.* **2012**, *3*, 443–446. [CrossRef]
33. Zhang, G.; Lan, Z.A.; Wang, X. Surface engineering of graphitic carbon nitride polymers with cocatalysts for photocatalytic overall water splitting. *Chem. Sci.* **2017**, *8*, 5261–5274. [CrossRef] [PubMed]
34. Lin, Y.; Liu, Y.; Li, Y.; Cao, Y.H.; Huang, J.N.; Wang, H.J.; Yu, H.; Liang, H.; Peng, F. Dual functional CuO_{1-x} clusters for enhanced photocatalytic activity and stability of a Pt cocatalyst in an overall water-splitting reaction. *ACS Sustain. Chem. Eng.* **2018**, *6*, 17340–17351. [CrossRef]
35. Niu, P.; Zhang, L.; Liu, G.; Cheng, H.M. Graphene-like carbon nitride nanosheets for improved photocatalytic activities. *Adv. Funct. Mater.* **2012**, *22*, 4763–4770. [CrossRef]
36. Peng, S.; Cao, Y.; Zhou, F.; Xu, Z.D.; Li, Y.X. CoP decorated with Co_3O_4 as a cocatalyst for enhanced photocatalytic hydrogen evolution via dye sensitization. *Appl. Surf. Sci.* **2019**, *487*, 315–321. [CrossRef]
37. Zhang, X.; Xie, X.; Wang, H.; Wang, H.; Zhang, J.J.; Pan, B.C.; Xie, Y. Enhanced photoresponsive ultrathin graphitic-phase C_3N_4 nanosheets for bioimaging. *J. Am. Chem. Soc.* **2013**, *135*, 18–21. [CrossRef] [PubMed]
38. Li, A.; Wang, T.; Li, C.; Huang, Z.Q.; Luo, Z.B.; Gong, J.L. Adjusting the reduction potential of electrons by quantum confinement for selective photoreduction of CO_2 to methanol. *Angew. Chem. Int. Ed.* **2019**, *58*, 3804–3808. [CrossRef]
39. Fajrina, N.; Tahir, M. A critical review in strategies to improve photocatalytic water splitting towards hydrogen production. *Int. J. Hydrogen Energy* **2019**, *44*, 540–577. [CrossRef]
40. Qiu, P.; Chen, H.; Jiang, F. Cobalt modified mesoporous graphitic carbon nitride with enhanced visible-light photocatalytic activity. *RSC Adv.* **2014**, *4*, 39969–39977. [CrossRef]
41. Cui, Y.; Ding, Z.; Fu, X.; Wang, X.C. Construction of conjugated carbon nitride nanoarchitectures in solution at low temperatures for photoredox catalysis. *Angew. Chem. Int. Ed.* **2012**, *51*, 11814–11818. [CrossRef] [PubMed]
42. Chen, G.; Si, X.; Yu, J.; Bai, H.Y.; Zhang, X.H. Doping nano-Co_3O_4 surface with bigger nanosized Ag and its photocatalytic properties for visible light photodegradation of organic dyes. *Appl. Surf. Sci.* **2015**, *330*, 191–199. [CrossRef]
43. Chen, G.L.; Guyon, C.; Zhang, Z.X.; Ognier, S.; Beem, J.; Tatoulian, M. The different structure characteristics of nanosized Co_3O_4 film crystallized by the annealing and plasma techniques. *Mater. Lett.* **2013**, *107*, 111–114. [CrossRef]
44. Makuła, P.; Pacia, M.; Macyk, W. How to correctly determine the band gap energy of modified semiconductor photocatalysts based on UV–Vis spectra. *Phys. Chem. Lett.* **2018**, *9*, 6814–6817. [CrossRef] [PubMed]
45. Wang, Y.; Zhu, C.; Zuo, G.; Guo, Y.; Xiao, W.; Dai, Y.X.; Kong, J.J.; Xu, X.M.; Zhou, Y.X.; Xie, A.M.; et al. 0D/2D Co_3O_4/TiO_2 Z-Scheme heterojunction for boosted photocatalytic degradation and mechanism investigation. *Appl. Catal. B Environ.* **2020**, *278*, 119298. [CrossRef]
46. Li, G.; Wang, B.; Zhang, J.; Wang, R.; Liu, H.L. Rational construction of a direct Z-scheme g-C_3N_4/CdS photocatalyst with enhanced visible light photocatalytic activity and degradation of erythromycin and tetracycline. *Appl. Surf. Sci.* **2019**, *478*, 1056–1064. [CrossRef]
47. Chen, M.; Wu, J.; Lu, C.; Luo, X.; Huang, Y.Q.; Jin, B.; Gao, H.X.; Zhang, X.W.; Argyle, M.; Liang, Z.W. Photoreduction of CO_2 in the presence of CH_4 over g-C_3N_4 modified with TiO_2 nanoparticles at room temperature. *Green Energy Environ.* **2020**, *6*, 938–951. [CrossRef]
48. Chang, X.; Wang, T.; Zhang, P.; Zhang, J.J.; Li, A.; Gong, J.L. Enhanced surface reaction kinetics and charge separation of p–n heterojunction $Co_3O_4/BiVO_4$ photoanodes. *J. Am. Chem. Soc.* **2015**, *137*, 8356–8359. [CrossRef] [PubMed]
49. Li, Y.; Xue, Y.; Tian, J.; Song, X.J.; Zhang, X.J.; Wang, X.Z.; Cui, H.Z. Silver oxide decorated graphitic carbon nitride for the realization of photocatalytic degradation over the full solar spectrum: From UV to NIR region. *Sol. Energy Mater. Sol. Cells* **2017**, *168*, 100–111. [CrossRef]